

A&A manuscript no.

(will be inserted by hand later)

Your thesaurus codes are:

3 (11.16.1 11.09.2 11.05.1 11.14.1 11.19.1)

An HST Surface Photometric Study of Ultraluminous Infrared Galaxies [★]

Z. Zheng^{1,5}, H. Wu^{1,5}, S. Mao², X.-Y. Xia^{3,5}, Z.-G. Deng^{4,5}, Z.-L. Zou^{1,5},

¹ Beijing Astronomical Observatory, Chinese Academy of Sciences, 100080 Beijing, P. R. China

² Max-Planck-Institut für Astrophysik Karl-Schwarzschild-Strasse 1, 85740 Garching, Germany

³ Dept. of Physics, Tianjin Normal University, 300074 Tianjin, P. R. China

⁴ Dept. of Physics, Graduate School, Chinese Academy of Sciences, 100039 Beijing, P. R. China

⁵ Beijing Astrophysics Center (BAC)[†], 100871, Beijing, P. R. China

Received, 1998; Accepted, 1998

Abstract. We study the surface photometry for 13 single-nucleus ultraluminous IRAS galaxies (ULIRGs), selected from a parent sample of 58 galaxies obtained in a Hubble Space Telescope snapshot survey. We find that these galaxies can be classified into three classes according to their surface photometry. The surface brightness profiles of the four objects in the first class are well fitted by the $R^{\frac{1}{4}}$ law. The isophotes are all diskly at $R \lesssim 1h^{-1}$ kpc, consistent with the molecular disks/rings found in nearby ULIRGs from CO observations. Each of the four galaxies in the second class has an inner $R^{\frac{1}{4}}$ component plus an outer extension. Remarkably all these four galaxies are Seyfert 1 galaxies with luminosities in the quasar regime and with relatively narrow permitted and strong FeII emission lines. The remaining five galaxies fall into the third class; these objects have surface brightness profiles that deviate to various degrees from the $R^{\frac{1}{4}}$ law; indeed, one is fitted perfectly by an exponential law. We also present new spectroscopic observations for some of these galaxies. We establish the redshift of IR 09427+1929 to be 0.284, instead of 0.149 as adopted in the literature. These observations firmly support the idea that merging of disk galaxies produce ellipticals. Our data also strongly suggest that the formation of QSOs may be an integral part of elliptical galaxy formation (at low redshifts).

Key words: Galaxies: photometry Galaxies: interactions Galaxies: elliptical Galaxies: Seyfert Galaxies: nuclei

1. Introduction

Ultraluminous IRAS galaxies (ULIRGs), characterized by their high far-infrared luminosities $L_{\text{IR}} > 10^{12}L_{\odot}$ (for $H_0 = 50 \text{ km s}^{-1} \text{ Mpc}^{-1}$), are the most luminous galaxies in the local universe (see Sanders & Mirabel 1996 for a review). Most ULIRGs show signs of interaction and/or merging. These processes are believed to trigger starbursts and central nuclear activities which in turn produce intense infrared emissions via dust absorption and re-emission. Some ULIRGs do not show prominent interaction signatures (at least from ground-based imaging), but these could be advanced mergers, as is the case for the ULIRGs with highest luminosities ($L_{\text{IR}} > 2.25 \times 10^{12}L_{\odot}$, for $H_0 = 50 \text{ km s}^{-1} \text{ Mpc}^{-1}$). These ULIRGs may represent an important stage in formation of QSOs and powerful radio galaxies, and may also present a primary stage in the formation of elliptical galaxies. (Sanders et al 1988a; Sanders & Mirabel 1996; Melnick & Mirabel 1990).

Although the ultimate fate of the ULIRGs is not yet fully understood, more and more observations show that the remnants of the mergers resemble elliptical galaxies or S0 galaxies. For example, the surface brightness profile of IRAS 20551-4250 is reasonably well fitted by the $R^{\frac{1}{4}}$ law (Johansson 1991). Arp 220 and NGC 6240, two nearest ULIRGs, both have densities, velocity dispersions and central surface brightness distributions consistent with the fundamental plane of elliptical galaxies (Doyon et al 1994). Baker & Clements (1997) investigated the old stellar population for 10 nearby ULIRGs based on deep near-infrared imaging and concluded that 8 out of 10 ULIRGs show signs of elliptical structure.

On the theoretical side, Toomre & Toomre (1972) first successfully reproduced the observed bridges and tails using restricted three-body simulations of two colliding disk galaxies. In 1977, Toomre put forward the hypothesis that all elliptical galaxies could be remnants of merged disk galaxies. Later simulations improved the spatial resolutions, explored more phase space of the encounter geome-

Send offprint requests to: Z. Zheng (zhengz@bac.pku.edu.cn)

[†] BAC is jointly sponsored by the Chinese Academy of Sciences and Peking University.

^{*} This research was based on observations obtained with the NASA/ESA *Hubble Space Telescope* through the Space Telescope Science Institute, which is operated by the Association of Universities for Research in Astronomy, Inc., under NASA contract NAS5-26555.

try and incorporated more realistic treatments of the progenitors, adding components such as bulges, massive dark matter haloes and gas; crude treatment of star formation is also attempted (e.g. White 1978; Farouki & Shapiro 1982; Negroponte & White 1983; Barnes 1992; Hernquist 1992; Heyl et al 1994; Barnes & Hernquist 1996; Weil & Hernquist 1996; Walker et al 1996; Mihos & Hernquist 1994). These simulations conclude that a wide range of initial conditions can result in the formation of early-type-like galaxies (see de Zeeuw & Franx 1991 for a review). Besides the global elliptical-like characteristics of the remnants of simulated mergers (e.g. the $R^{\frac{1}{4}}$ law of the surface brightness profile), some simulations also attempt to reveal the fine structure of the remnants such as the shape of the isophote, loops, shells and tails (see e.g. Heyl et al 1994; Springel & White 1998). As mergers of galaxy pairs may not account for all observed properties of ellipticals, multiple mergers have been considered (Mamon 1987, Barnes 1984, Barnes 1985, Barnes 1989, Schweizer 1989; Weil & Hernquist 1996); multiple merging may occur in compact groups such as those found by Hickson (1982, 1993).

While the simulations indicate that merging of two or more disk galaxies can easily lead to the formation of ellipticals, it is clearly important to test these predictions empirically. For this purpose, ULIRGs are ideal since they are closely related to galaxy merging and interactions (e.g., Murphy et al 1996, Clements et al 1996). In this paper, we analyze the surface photometry for 13 ULIRGs observed with the Hubble Space Telescope (HST) Wide Field Planetary Camera 2 (WFPC2), and examine whether their profiles resemble the $R^{\frac{1}{4}}$ law, as one would expect if they ultimately form elliptical galaxies. The resolution of HST provides us a powerful way to study the inner profiles and the fine structure details in these galaxies. We will also address the important question whether the surface photometry of these galaxies are associated with the central active galactic nuclei (AGN) phenomenon. The structure of the paper is as follows. In section 2, we describe how we select our ULIRG sample. Data reduction including surface photometry is described in Section 3. In Section 4, we classify these galaxies according to their surface brightness profiles. In Section 5, we discuss the spectroscopic properties of these galaxies, using both newly obtained spectra and data from the literature. In Section 6, we summarize and discuss the implications of our results. Throughout this paper we adopt an Einstein-de Sitter universe ($\Omega_0 = 1$) and denote the Hubble constant as $H_0 = 100h \text{ km s}^{-1} \text{ Mpc}^{-1}$. Since our objects are at relatively low redshift ($z \lesssim 0.35$), the assumption about the density parameter (Ω_0) is not critical, and $1''$ corresponds to roughly $1h^{-1} \text{ kpc}$ ($z/0.1$) for $z \lesssim 0.4$.

2. Sample Selection

In this study, we use archive images from an HST snapshot survey of ultraluminous IRAS galaxies (Borne et al 1998).

This snapshot survey was taken using the WFPC2 in the I bandpass (F814W). The objects observed were mainly selected from the following samples: the bright samples of Sanders et al (1988a,b) and Melnick & Mirabel (1990), and the QDOT sample (Leech et al 1994; Lawrence et al 1999). For each target in this survey, two 400s exposures were taken. Most of target galaxies are centered on the Wide Field Camera chip 3 (800×800 pixels, $0.0996''$ per pixel) and a few in the Planetary Camera chip (800×800 pixels, $0.0455''$ per pixel). For details of this survey, see Borne et al (1998). In total, there are 58 images available to us from March 1996 to Jan. 1997 (except that IR 10026+4347 was taken in May 1997). The redshifts of these objects range from 0.04 to 0.35.

Table 1. Journal of Observations

Target Name	RA(2000)	Dec(2000)	Date
IR 09427+1929	09:45:29.1	19:15:50.0	23/05/96
IR 17432-5157	17:47:09.9	-51:58:44.0	27/10/96
IR 23140+0348	23:16:35.2	04:05:17.0	03/09/96
IR 04025-8303	03:57:11.3	-82:55:16.0	02/07/96
IR 00509+1225	00:53:34.8	12:41:36.1	29/08/96
IR 00276-2859	00:30:04.1	-28:42:25.6	05/10/96
IR 02055+0835	02:08:06.7	08:50:03.6	05/10/96
IR 10026+4347	10:05:41.9	43:32:39.4	01/05/97
IR 14378-3651	14:40:59.4	-37:04:33.2	02/09/96
IR 10559+3845	10:58:39.3	38:29:06.4	19/06/96
IR 20176-4756	20:21:11.1	-47:47:07.1	28/09/96
IR 09039+0503	09:06:34.1	04:51:28.3	17/11/96
IR 23242-0357	23:26:50.2	-03:41:05.5	24/08/96

The near infrared observation (F814W) minimizes the effect of the absorption by gas and dust in the target galaxies because the dust extinction at longer wavelengths is smaller. Moreover, near infrared imaging is not sensitive to young stellar populations. The I-band imaging is therefore more suitable for our primary goal of understanding how the old stellar populations relax dynamically during the merging process.

The ULIRGs in the Borne et al (1998) sample exhibit a variety of morphologies. Some have only a single nucleus while others have two or multiple nuclei and display complex and disturbed configurations. These morphologies are likely connected to different stages of merging and interaction. In this paper, we will focus on studying properties of the late-products of merging and relaxation, therefore we choose a subsample of galaxies that are dominated by a single nucleus; these single-nucleus galaxies are selected by checking the contour plot for each source. The targets in our sample all show merging features, such as tidal tails, plumes, shells and other fine structures. The galaxies selected through this way are probably all mergers at the late stage of interacting/merging (§4, see also Wu et

al 1998). In total, 13 targets are chosen out of the 58 images. The journal of observations for these targets is listed in Table 1.

3. Data Reduction

All observations were preprocessed “on the fly” through the standard Space Telescope Science Institute pipeline as described by Holtzman et al (1995). The images were calibrated (including bias subtraction and flat fielding) with the most up-to-date version of the routine reference files provided by the Institute at the time the images were taken. After correction of hot pixels, our image processing mainly include cosmic-ray removal and sky subtraction, which we describe below.

3.1. Cosmic-ray Cleaning

With its high altitude, HST is free of atmospheric seeing effects, however this also means that it is much more susceptible to cosmic ray hits than ground-based telescopes. So it is essential to carefully remove the cosmic rays.

Since for each of our object there are two 400s exposures that are in general well aligned, the cosmic-ray removal is relatively straightforward. We use the standard IRAF task “combine” with a (conventional) 3σ clipping threshold to detect the cosmic-rays. The cosmic-ray free images are then co-added. The combined image has a higher signal-to-noise ratio than each single image, usually by a factor of $\sqrt{2}$ except for some individual pixels.

3.2. Sky Subtraction

The background of each combined image was fitted by performing the IRAF task “imsurfit”. Since the field of view for the Wide Field Camera is small (about $80'' \times 80''$), it is reasonable that the sky background has a relatively small variation across the field. After several trials, we found that it is sufficient to fit the sky background using a two-dimensional second-order Legendre function, i.e., a “declined plane”. Some rectangular regions (usually each includes more than 2000 pixels) were chosen from the combined image to sample the sky background. The median value of each region was used for the fitting.

The sky-subtracted image is then ready for photometric purposes.

3.3. Surface Photometry

We perform the surface photometry using the ISOPHOTE package in STSDAS in the IRAF environment.

Foreground stars and diffraction spikes caused by bright stars or central nuclei in each image were carefully masked out to eliminate their effect on the photometry. We use the SExtractor galaxy photometry package (v1.2b10b) (Bertin & Arnouts 1996) to help identify the

stars. A circular region and a triangular region are used to mask a star and a spike, respectively. Pixels inside these regions are given zero weighting in the ellipse fitting procedure which we describe below.

3.3.1. Isophote Ellipse Fitting

For all galaxies, the IRAF task “ellipse” was used to derive the isophotal morphological parameters.

The “ellipse” task fits ellipses which best reproduce the observed isophotes of an image (Jedrzejewski 1987). The best parameters are found by an iterative procedure. In each run of the isophote fitting, a number of parameters are used to describe the fitted ellipse. These include the ellipse center (x_0, y_0) , semi-major axis a , ellipticity ϵ ($\epsilon \equiv 1 - b/a$, where b is the semi-minor axis), position angle ϕ (the azimuthal angle of the major axis, measured counter-clockwise from the $+y$ direction in the image here). To describe the deviation of isophotes from perfect ellipses, the difference between the isophotal radius and the best ellipse fit is usually expanded in Fourier series. The coefficient of $\cos 4\theta$ term in the expansion, B_4 , is given particular importance in describing the deviation (e.g. Carter 1977, Jedrzejewski 1987; Kormendy & Bender 1996): if B_4 is positive, the isophote is more elongated along the major axis than the best fitting ellipse and is said to be *disky*; on the other hand, if B_4 is negative, the isophote will appear rectangular (*boxy*). The intensity around each isophote is measured by averaging the flux azimuthally. The ellipse center, ellipticity and position angle are allowed to change in this work for two reasons: First, ellipticity changes and isophote twisting (i.e. changes of position angle) have already been noticed in elliptical galaxies. Second, our sample mainly includes interacting/merging galaxies. Behavior of the changes in the parameters may reveal interesting structure details.

3.3.2. Fitting the Surface Brightness Profile

In order to address the questions mentioned in the introduction, we checked the one-dimensional surface brightness profiles obtained through isophote ellipse fitting.

We fit the radial profiles with a Sérsic (1968) law (Marleau & Simard 1998):

$$I(r) = I_e \exp(-b[(\frac{R}{R_e})^{1/n} - 1]), \quad b = 1.9992n - 0.3271, \quad (1)$$

where $I(R)$ is the surface brightness at radius R , and R_e is the effective radius within which half of the light is enclosed (Capaccioli 1989). The de Vaucouleurs $R^{\frac{1}{4}}$ profile, which is usually used to describe elliptical galaxies and bulges, is a special case of (1) with $n = 4$, and the exponential profile, which is used to describe galactic disks, is also a special case with $n = 1$.

Table 2. Properties for the Ultraluminous IRAS Galaxies

Target Name	Redshift	$M_I - 5 \log h$	$\text{Log}(h^2 \cdot L_{\text{far}} / L_{\odot})$	$R_e (h^{-1} \text{kpc})$	Spectral Type	Class	Comments
IR 09427+1929	0.28400	<-23.21	12.01	2.75	Sy1 ^o	1	Strong FeII
IR 17432-5157	0.17500	-21.11	11.73	4.99	LINER ^s	1	
IR 23140+0348	0.21980	-22.94	11.79	2.47	LINER ^o	1	Radio Galaxy
IR 04025-8303	0.13660	<-22.41	11.55	0.94	Sy1 ^l	1	
IR 00509+1225	0.06114	<-22.72	11.21	2.69	Sy1 ⁿ	2	Strong FeII
IR 00276-2859	0.28000	<-23.70	12.04	3.25	Sy1 ⁿ	2	Strong FeII
IR 02055+0835	0.34500	<-23.31	12.37	0.80	Sy1 ^l	2	Strong FeII
IR 10026+4347	0.17800	<-23.11	11.59	0.84	Sy1 ^l	2	Strong FeII
IR 14378-3651	0.06760	-21.17	11.72	-	LINER ^k	3	
IR 10559+3845	0.20660	-22.32	11.74	-	HII ^s	3	
IR 20176-4756	0.17810	-21.51	11.81	-	not AGN ^l	3	
IR 09039+0503	0.12500	-21.80	11.70	-	LINER ^o	3	
IR 23242-0357	0.18900	-21.64	11.52	-	HII ^o	3	

ⁿ NED; ^s Spectra of QDOT; ^l Lawrence et al 1999; ^k Kim et al 1998; ^o Our observation

4. Results

Table 2 gives the properties for these galaxies, including their redshifts, magnitudes, infrared luminosities and spectral classifications. The integrated apparent WFPC2 magnitude is obtained from aperture photometry in the sky-subtracted and star-masked image using the formula from Holtzman et al (1995); the apparent magnitude is then converted into absolute magnitude using luminosity distances for our cosmology (no k-correction has been applied). In the case of saturated images, only upper limits (in absolute magnitude) are given. Figs. 1-13 (left panels) show the HST images for all thirteen galaxies. Each image has 750×750 pixels, corresponding to $74.5''$ on a side. The middle panels show the contour levels for a smaller region centered on each target, highlighting its environments. The right panels show the variations of the surface brightness, ellipticity, position angle and B_4/a as a function of $R^{\frac{1}{4}}$. From the radial surface brightness profiles we classify these galaxies into three classes:

- I. The first class includes 4 galaxies; the surface brightness of each galaxy in this class is well fitted by the $R^{\frac{1}{4}}$ law with some small deviations at $\sim h^{-1}$ kpc. These four galaxies have round appearances.
- II. The second class includes 4 galaxies. The surface brightness profile for each galaxy in this class has two components: an inner $R^{\frac{1}{4}}$ component and an outer component. There is a bright central nucleus in each of these galaxies. The best-fit effective radii (for the $R^{\frac{1}{4}}$ component) for class I and II galaxies are given in Table 2.
- III. The remaining 5 galaxies fall into the third class. These galaxies have surface brightness profiles that deviate significantly from the $R^{\frac{1}{4}}$ law.

In the following, we will discuss the properties of these three classes in detail.

4.1. Class I

Four galaxies (**IR 09427+1929**, **IR 17432-5157**, **IR 23140+0348**, **IR 04025-8303**) belong to class I. The surface brightness profiles for these galaxies are well described by the $R^{\frac{1}{4}}$ law, from the very inner part to the outer part as shown in Fig. 1 to Fig. 4. For IR 17432-5157, the fit is reasonable from $0.5 h^{-1}$ kpc to $9.2 h^{-1}$ kpc; for IR 23140+0348, the fit is excellent out to $13 h^{-1}$ kpc. Another common characteristic of these galaxies is that they have round appearance. For each galaxy, the *maximum* ellipticity of the isophotes is less than 0.30. The ellipticities at the effective radius are even smaller. They are only 0.2, 0.1, 0.1, and 0.1 for IR 09427+1929, IR 17432-5157, IR 23140+0348, IR 04025-8303, respectively.

However, there are slight deviations from the exact $R^{\frac{1}{4}}$ law. Small excesses over the best-fitted curve can be seen in all surface brightness profiles (right panels in Figs. 1-4) at $\sim (1-3)h^{-1}$ kpc. The bump position in each galaxy coincides with the maximum of the ellipticity ϵ . This coincidence reflects small structures in these galaxies. Furthermore, it is very interesting that all four galaxies have disk isophotes ($B_4 > 0$) in the very inner regions ($\leq 1 h^{-1}$ kpc), and the position angle change is very large, ($\sim 100^\circ$ for some galaxies). Carollo et al (1997) analysed HST WFPC2 images for 15 elliptical galaxies. In both F555W and F814W filters, the position angle changes are usually less than 20° . Therefore it appears that although the light profile is described by the $R^{\frac{1}{4}}$ law, the ellipses still show substantial twists.

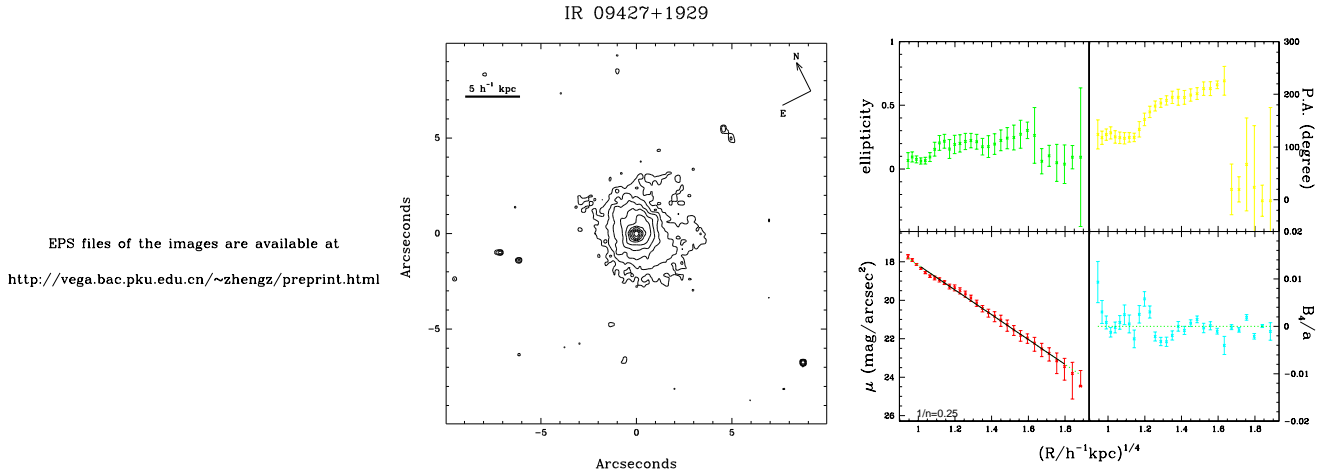


Fig. 1. The left panel shows the HST Wide Field Camera image for IR 09427+1929 (the object labeled as G0). The image shown is $74.5''$ on a side. Three additional galaxies (G1, G2 and G3) are within the field. The ellipse shows the error box of the IRAS position (cf. §5.1). The middle panel shows the contours centered on IR 09427+1929; the contour levels are 2, 4, 8, 16, 32, 64, 128, 256, 512, 1024 ADU, respectively. The thick horizontal bar indicates a scale of $5h^{-1}$ kpc. The north and east directions are indicated at the top right in the middle panel. The right panels show the variations of the ellipticity, position angle, surface brightness, and B_4/a (see §3.3) as a function of $R^{1/4}$. The best $R^{1/4}$ fit to the surface brightness profile is given by the straight line.

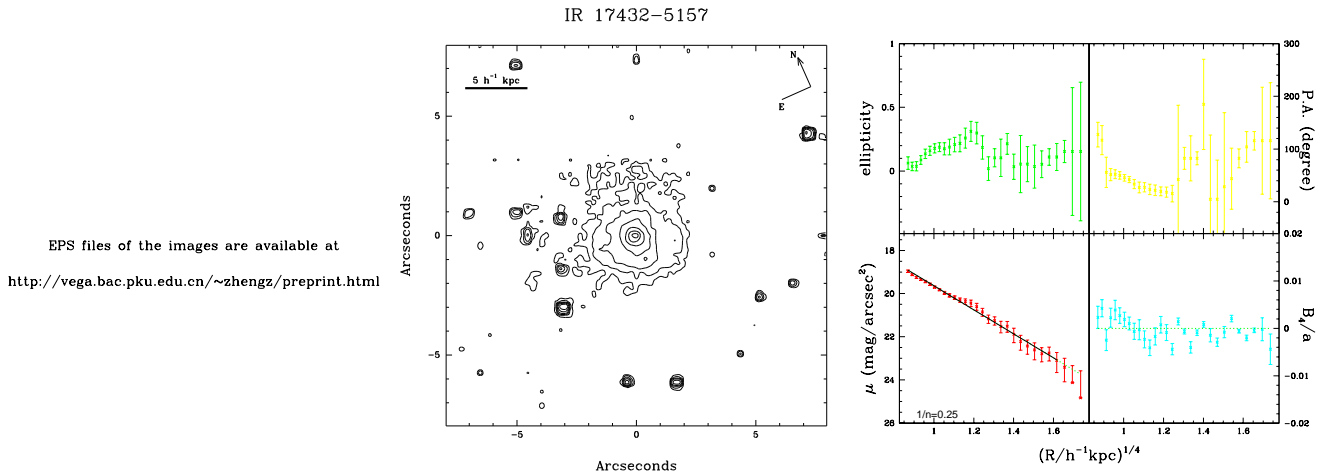


Fig. 2. Same as in Fig. 1, for IR 17432-5157. At least one additional galaxy are within the field. Due to its low Galactic latitude (-12°), many stars are also present. The contour levels are 1.9, 3.8, 7.6, 15.2, 30.4, 60.8, 121.6, 243.2, 486.4 ADU, respectively.

From Figs. 1-4, it can be seen that all four galaxies exhibit signatures of merging such as short tails, plumes in their outer parts. Except for IR 23140+0348, all the other galaxies have some other galaxies within the same field of view, but these could be due to chance alignment (see Section 5). The round appearance of these galaxies provides a clue to the merging environment. Numerical simulations (e.g. Weil & Hernquist 1996) found that remnants of multiple mergers are more round than the mergers from pair stellar disks (when projected onto the sky). So the round appearance of the class I galaxies suggests that they may be remnants of multiple mergers. Such a possibility is supported by the high percentage of multiple nuclei galaxies

in our parent sample of 58 galaxies. About 50% of these have more than three nuclei. Furthermore, for some of the double-nucleus galaxies, each of the two merging nuclei could contain a pair of galactic nuclei in high-resolution images, similar to Arp 220 (Taniguchi & Shioya 1998). Therefore, the percentage of the multiple-nucleus galaxies is likely higher than 50% for our sample, supporting the notion that ULIRGs may preferentially reside in groups of galaxies (Wu et al 1998).

The physical significance of the disk isophotes at the inner radius ($\leq 1h^{-1}$ kpc) and the excesses at ($\sim 3h^{-1}$ kpc) is not clear. Multiple-waveband observations of ULIRGs reveal the presence of massive starbursts in

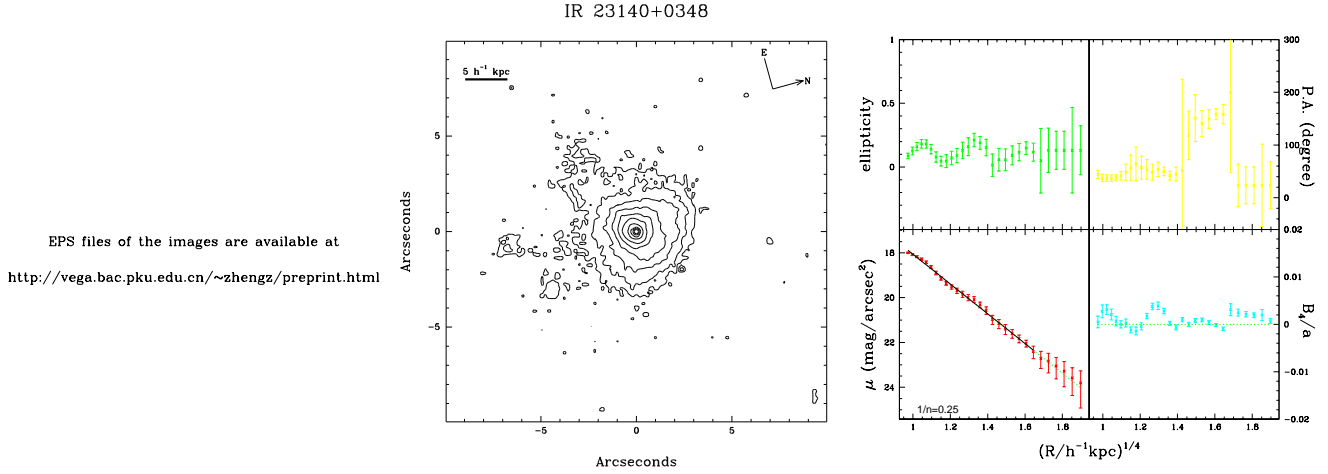


Fig. 3. Same as in Fig. 1, for IR 23140+0348 (labeled as G0). Faint features are visible around G0. The contour levels are 1.64, 3.28, 6.56, 13.12, 26.24, 52.48, 104.96, 209.92, 419.84, 839.68, 1679.36 ADU, respectively.

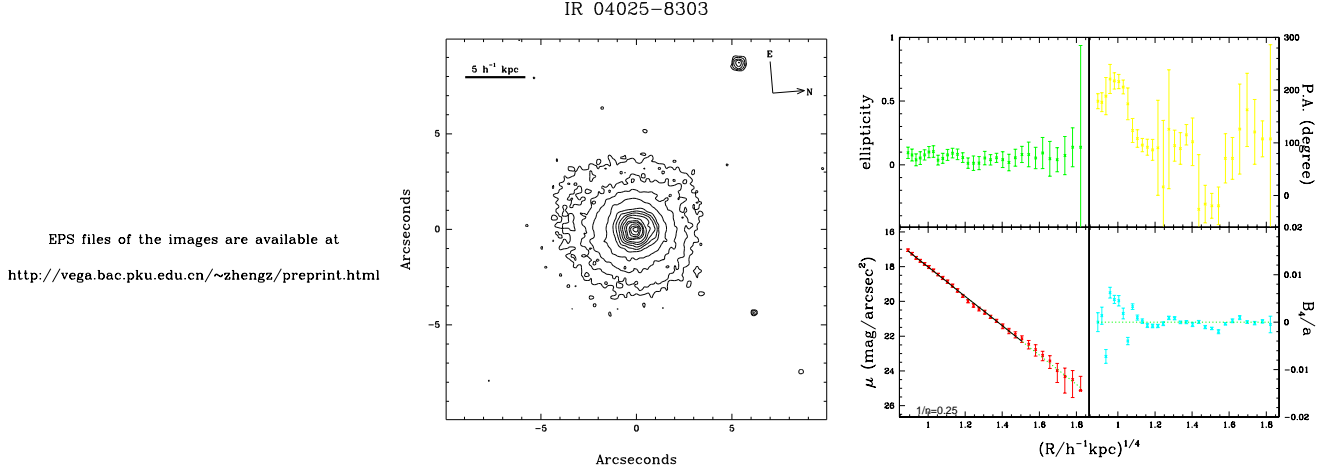


Fig. 4. Same as in Fig. 1, for IR 04025-8303. At least one additional galaxy (G1) is within the field. The contour levels are 1.55, 3.1, 6.2, 12.4, 24.8, 35, 49.6, 70, 99.2, 150, 198.4, 396.8, 793.6, 1587.2, 3174.4 ADU, respectively.

a molecular ring or disk at several hundred pc to kpc in the circumnuclear regions (e.g., Downes & Solomon 1998). The positions of the inner disk isophotes may reflect the presence of such small disks at the center. Such nuclear disks are also found in numerical simulations where gas is driven inward to the central kpc region and cool efficiently at early stage of galactic encounters (Icke 1985; Noguchi 1988). Therefore, the inner “disky” structure could be the relics of nucleus starburst rings or disks. The significance of bumps at $\sim 3h^{-1}$ kpc is less clear, since even “normal” elliptical galaxies do not follow the $R^{\frac{1}{4}}$ law perfectly (e.g., Saglia et al 1997). These departures could be produced in the merging process by tidal force and/or dynamical friction.

4.2. Class II

Figs. 5-8 show the four galaxies in class II. Surface brightness profiles of all these galaxies can be fitted by the $R^{\frac{1}{4}}$

law from $\sim 1h^{-1}$ kpc out to $\sim 5h^{-1}$ kpc. The outer parts of these galaxies show clear excess over the $R^{\frac{1}{4}}$ law. We have tried a two-component fitting with an inner $R^{\frac{1}{4}}$ component and an outer exponential component. We find, however, that the fitting is unsatisfactory, meaning that the outer extension is more complex than a simple exponential. Disky isophotes are found in the inner region of each galaxy. However, this is clearly an artefact caused by the saturated central nuclei, since the diagonals of the quasi-diamond shaped isophotes are almost along the diagonals of the images.

Although our classification of these galaxies are based purely on their surface brightness profiles, remarkably, we found that all the four galaxies host luminous bright nuclei and are saturated in the frames. All the galaxies were classified as Seyfert 1 galaxies spectroscopically (Lawrence et al. 1999; Vader & Simon 1987; Moran et al 1996), and all have luminosities in the QSO regime. For details, see Sect. 5.2.

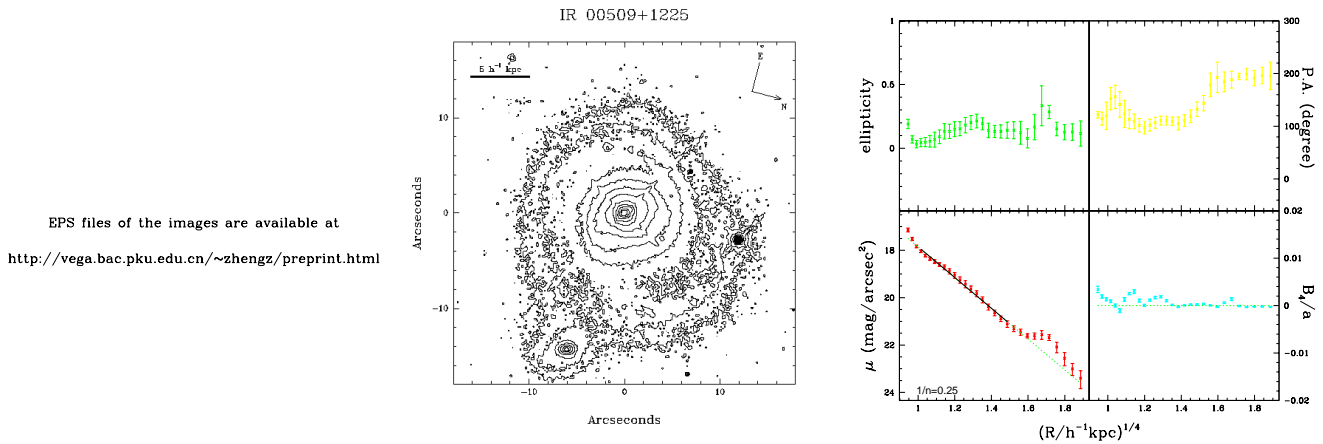


Fig. 5. The left panel shows the HST Wide Field Camera image for IR 00509+1225 (the object labeled as G0). The image shown is $74.5''$ on a side. A satellite galaxy (G1) and a foreground star S1 are visible. The middle panel shows the contours centered on IR 00509+1225; the contour levels are 1.7, 3.4, 6.8, 13.6, 27.2, 54.4, 108.8, 217.6, 435.2, 870.4, 1740.8 ADU, respectively. The thick horizontal bar indicates a scale of $5h^{-1} \text{ kpc}$. The north and east directions are indicated at the top right in the middle panel. The right panels show the variations of the ellipticity, position angle, surface brightness, and B_4/a (see §3.3) as a function of $R^{1/4}$. The best $R^{1/4}$ fit to the surface brightness profile is given by the straight line.

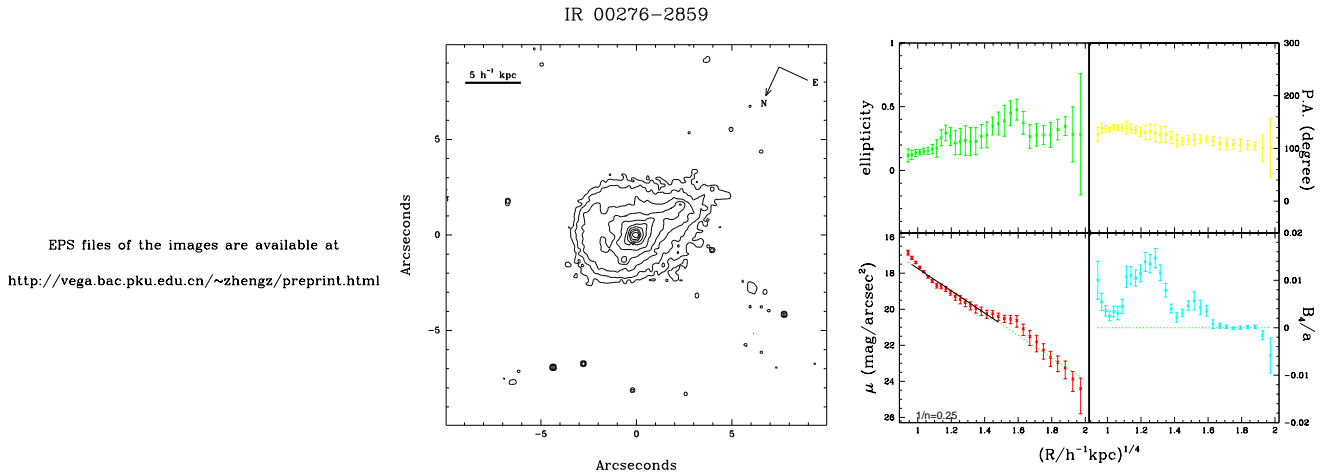


Fig. 6. Same as in Fig. 5, for IR 00276–2859. A number of galaxies (G1–G5) and a star (S1) are within the field. The contour levels are 1.65, 3.3, 6.6, 13.2, 26.4, 52.8, 105.6, 311.2, 622.4, 1244.8, 2489.6 ADU, respectively.

IR 00509+1225 It has a small galaxy with a projected distance of $13h^{-1} \text{ kpc}$ away to the west. Two armlike features are clearly visible. The optical feature from ground based deep observation looks like that of Mrk 231 (for details see Surace et al 1998). These armlike features could be tidal tails resulting from merging.

IR 00276–2859 There are a number of small galaxies within the same field. In the contour plot, a small galaxy (G1) to the southeast can be detected. G1 causes the outer contours of IR 00276–2859 to protrude in its direction, indicating that these two galaxies are physically interacting.

IR 02055+0835 This galaxy has an extension to the west. Two objects G1 and G2 are within the same

field. Both objects are within a projected distance of $20h^{-1} \text{ kpc}$ and could be physically associated with the IRAS galaxy. Many small and fainter objects are also visible within $20''$.

IR 10026+4347 This galaxy is an IR QSO and is potentially a member of one important class of transition objects. Detailed discussions for this object will be found in Xia et al (1999).

4.3. Class III

The five galaxies in this class have different surface brightness profiles, and so we discuss them in turn.

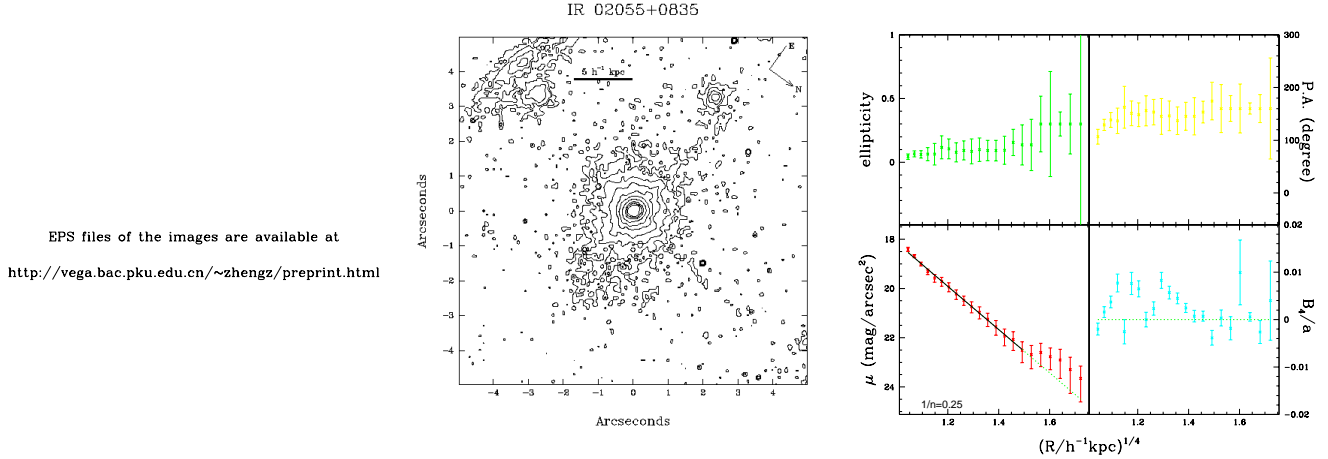


Fig. 7. Same as in Fig. 5, for IR 02055+0835. The contour levels are 1.7, 3.4, 6.8, 13.6, 27.2, 54.4, 108.8, 217.6, 435.2, 870.4 ADU, respectively. Two nearby objects (G1 and G2) are clearly visible.

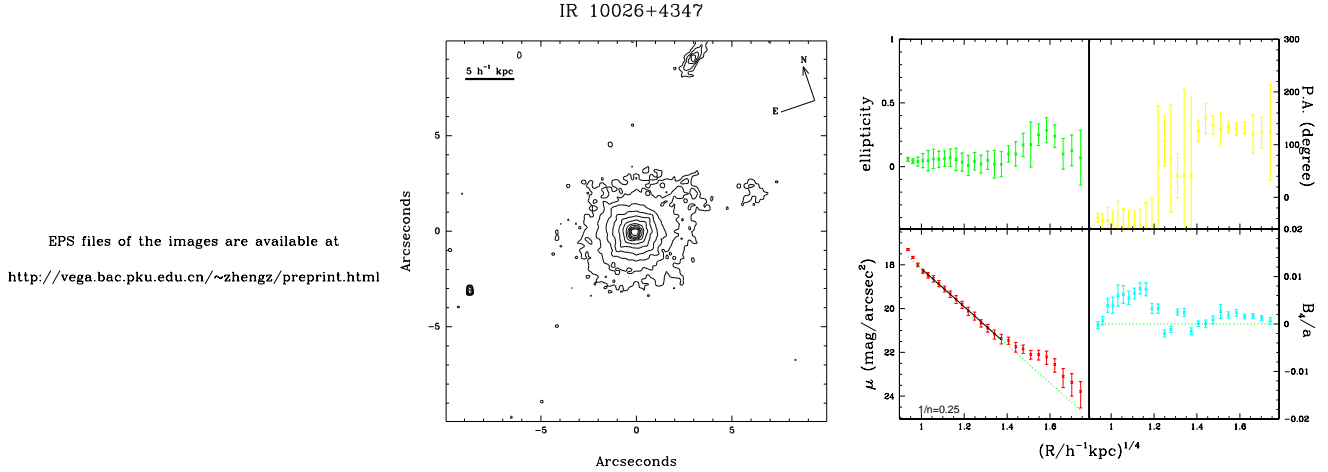


Fig. 8. Same as in Fig. 5, for IR 10026+4347. The contour levels are 1.75, 3.5, 7, 14, 28, 56, 112, 224, 448, 896, 1792 ADU, respectively.

IR 14378–3651 It is a galaxy with an asymmetric extension, being more diffuse to the northwest, as can be seen in Fig. 9. A small galaxy (G1) is visible about $4h^{-1}$ kpc (projected) to the southwest. This galaxy is still within the envelope of IR 14378–3651 and could be physically associated with IR 14378–3651. A ripple-like material can be separated from the southeast part of the extension. A loop structure can be seen in the inner part which is similar to spiral arms. The isophotes are disk-like within $1h^{-1}$ kpc. The surface brightness profile of this source deviates from the $R^{1/4}$ law. If we fit it with the $R^{1/4}$ law, we find a bump at $1.5h^{-1}$ kpc and a dent at $2.8h^{-1}$ kpc. The inner bump is related to the inner arms. Apart from the outer part, this galaxy has a round appearance ($\epsilon < 0.3$). The ripples, loop structures and the deviation from the $R^{1/4}$ law suggest that IR 14378–3651 is a merging galaxy and is still relaxing towards the $R^{1/4}$ light distribution.

IR 10559+3845 From Fig. 10, IR 10559+3845 appears to have two nearly symmetric diffuse tails. NICMOS observations reveal two very close nuclei (Borne et al 1998), indicating that this galaxy is a merging galaxy as well. The position angle of the major axis continuously changes by about 120 degrees from the center to the outer part; the position angle change in the inner part is more gradual than that in the outer part. The ellipticity of the inner isophotes is smaller (about 0.3) than the outer value (about 0.5). The center of the inner isophotes offsets to the south with respect to that of the outer ones. The merging process appears not yet complete for this galaxy.

IR 20176–4756 From both image and surface brightness profile (see Fig. 11), this galaxy appears to have been well relaxed. Remarkably, the surface brightness profile can be well fitted by a single exponential, ranging from $0.8h^{-1}$ kpc to $9.5h^{-1}$ kpc. The central part

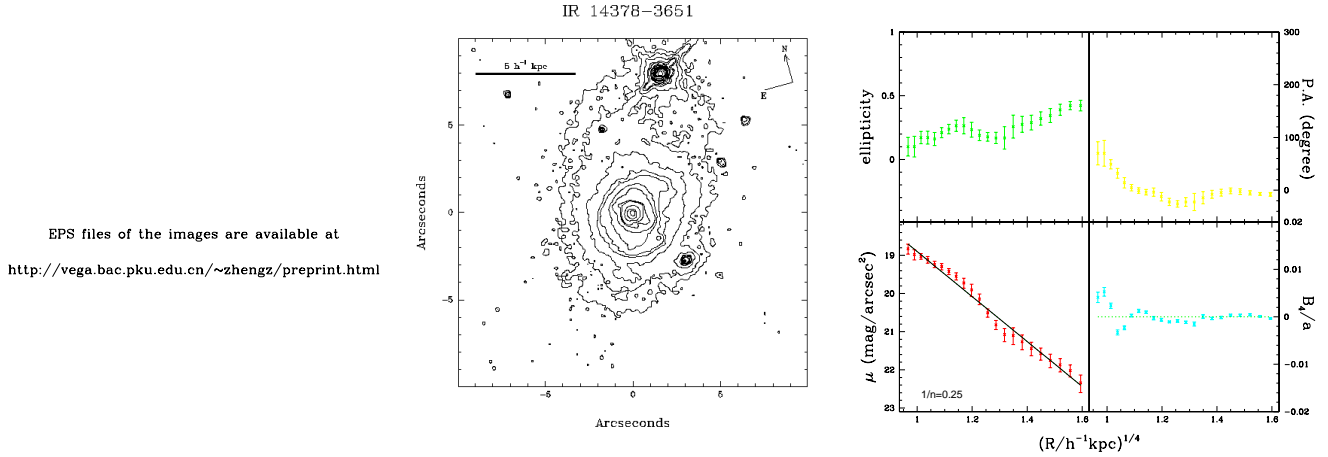


Fig. 9. The left panel shows the HST Wide Field Camera image for IR 14378–3651 (the object labeled as G0). The image shown is $74.5''$ on a side. A satellite galaxy (G1) and a foreground star S1 are visible. The middle panel shows the contours centered on IR 14378–3651; the contour levels are 1.9, 3.8, 7.6, 15.2, 20, 30.4, 40, 60.8, 70, 121.6, 243.2, 486.4, 972.8, 1943.6 ADU, respectively. The thick horizontal bar indicates a scale of $5h^{-1} \text{ kpc}$. The north and east directions are indicated at the top right in the middle panel. The right panels show the variations of the ellipticity, position angle, surface brightness, and B_4/a (see §3.3) as a function of $R^{1/4}$.

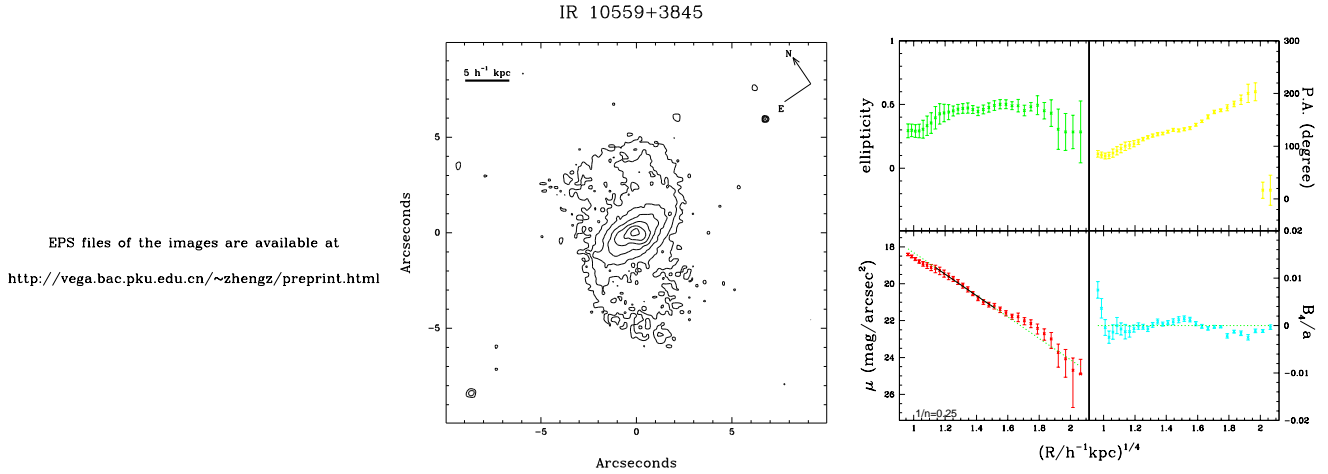


Fig. 10. Same as in Fig. 9, for IR 10559+3845. The contour levels are 1.7, 3.4, 6.8, 13.6, 27.2, 54.4, 108.8, 217.6, 435.2 ADU, respectively.

($\leq 1.4h^{-1} \text{ kpc}$) has boxy isophotes. On the other hand, there still exist merger signatures, such as a loop structure (or inner arms) in the inner region, fan-like protrusion and thick tail-like material at the outer region (marked with an arrow in the image). The most significant isophotal feature of IR 20176–4756 is that the position angle gradually decreases by about 180° . We speculate that the central boxy isophotes and isophotal twists may be caused by a central bar.

IR 09039+0503 This galaxy has a remarkable morphology as shown in Fig. 12. A thick and luminous tail emerges from the north and bends to the south with a total length of about $\sim 15h^{-1} \text{ kpc}$. Two short tails locate to the south and northwest, respectively. A closer look reveals that this galaxy has two very

close nuclei, which gives rise to the boxy isophotes within $1.2h^{-1} \text{ kpc}$. Although the central parts of the two galaxies have almost merged together, the galaxy is still far from complete relaxation and the surface brightness profile deviates significantly from the $R^{1/4}$ law. There are many small and faint objects within $30''$ of the source. It would be interesting to determine the redshifts of these small galaxies to see whether they are physically associated with the source.

IR 23242–0357 It has a surface brightness profile similar to that of the second class, it has an inner component satisfying $R^{1/4}$ law and a more extended outer component. The primary difference is that this galaxy has a fainter nucleus. The inner region has two fan structures which cause the boxy isophotes at radius

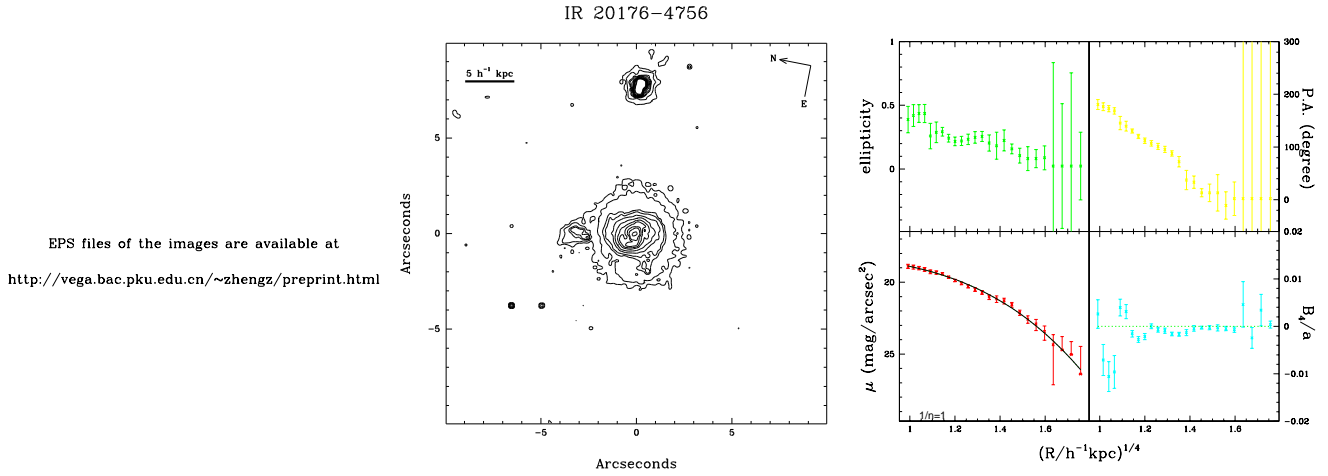


Fig. 11. Same as in Fig. 9, for IR 20176-4756. The contour levels are 1.75, 3.5, 7, 9, 14, 20, 28, 35, 45, 56, 90, 112 ADU, respectively. An excellent exponential fit to the surface brightness profile is also plotted. The arrow marks the protrusion and and thick tail-like material in the outer region.

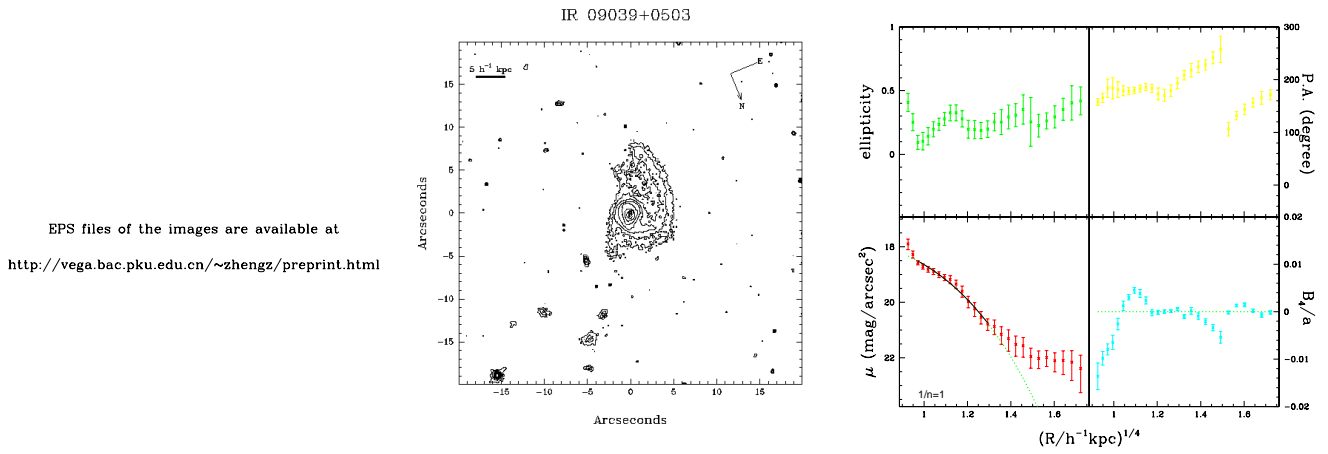


Fig. 12. Same as in Fig. 9, for IR 09039+0503. The contour levels are 1.77, 3.54, 7.08, 14.16, 28.32, 56.64, 113.28, 200, 226.56 ADU, respectively. An exponential fit to the surface brightness profile is also plotted.

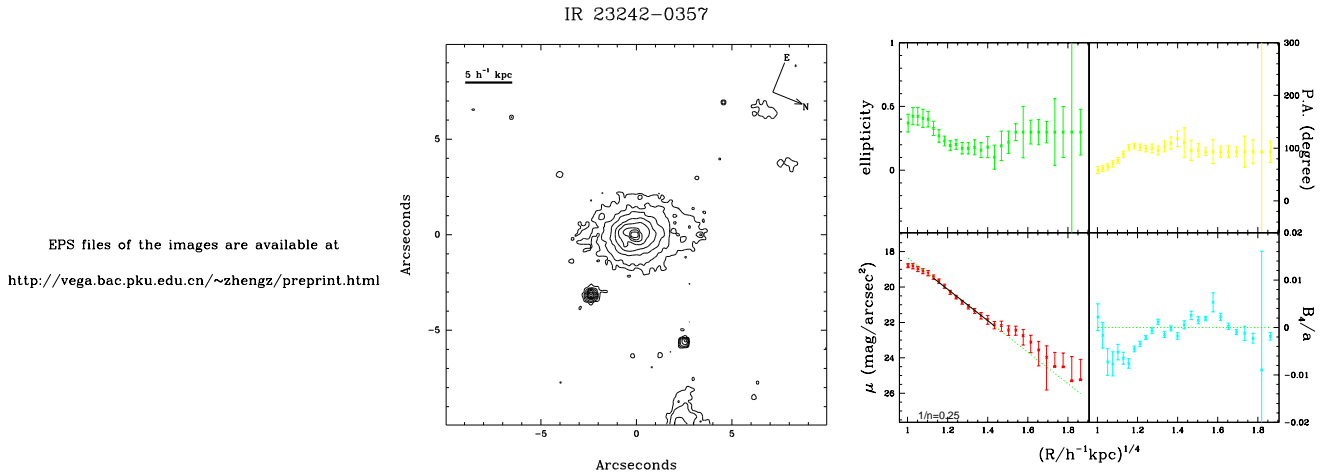


Fig. 13. Same as in Fig. 9, for IR 23242-0357. The contour levels are 1.7, 3.4, 6.8, 13.6, 27.2, 54.4, 108.8, 217.6, 435.2, 870.4 ADU, respectively. There are four other galaxies (G1-G4) within the field. The best $R^{\frac{1}{4}}$ fit to the surface brightness profile is given by the straight line.

$\leq 2.8h^{-1}$ kpc). The galaxy protrudes to the north-east and has a faint and slim spiral tail around it in the south. There are also four fainter galaxies (G1-G4) within the field, indicative of a group environment. Many fainter objects can be found within $15''$ of the source.

To summarize, the five galaxies in class III have diverse appearances, including one (IR 14378–3651) with a close double nuclei. Their surface brightness profiles deviate to different degrees from the $R^{\frac{1}{4}}$ law, with IR 20176–4756 fitted well by an exponential. IR 23242–0357 is similar to the objects in class II except that it has a fainter nucleus. We will return to the issue of the connection between the three classes of objects in the last section.

5. The Optical Spectroscopic Properties

Our studies so far have concentrated on the photometric properties of our sample galaxies. Clearly it is important to explore the spectroscopic properties of these galaxies in order to further understand these three classes of galaxies. In order to address this question and also to understand the possible group environment which we alluded to in Section 4, we have carried out spectroscopic observations from Dec. 20 to Dec. 23, 1998 using the 2.16m telescope at the Xinglong Station of Beijing Astronomical Observatory. We have observed IR 23140+0348, IR 09427+1929, IR 09039+0503 and IR 23242–0357, using a Zeiss universal spectrograph mounted on the 2.16m telescope. A Tektronix 1024×1024 CCD was used giving a wavelength coverage of 4100Å to 9100Å with a grating of 200Å/mm. The spectral resolutions are 9.3Å (2 pixels). Wavelength calibration was carried out using a He-Arg lamp; the resulting wavelength accuracy is better than 1Å. KPNO standard stars were observed to perform flux calibrations.

In the following section, we will present our observational results together with data available in the literature, such as Kim et al (1998) and Lawrence et al (1999), for these three classes of objects.

5.1. Class I

The spectrum of IR 23140+0348 is shown in Fig. 14. As can be seen from this figure, there are strong emission lines, as well as obvious 4000Å break (redshifted to ~ 4900 Å), G-band and possible CaII K and H absorption features. The Balmer absorptions are marginal in this low signal-to-noise ratio spectrum. From the emission line ratios and the classification criteria (Veilleux et al 1995; Osterbrock et al 1989), IR 23140+0348 can be classified as a LINER.

Compared with the “E+A”-like spectrum of ULIRGs FF J1614+3234 and TF J1020+6436 (Tran et al 1999; Breugel 1999; see also Dressler & Gunn 1983), the Balmer absorption line features of IR 23140+0348 is weaker. Nevertheless, the spectral features resemble each other and it

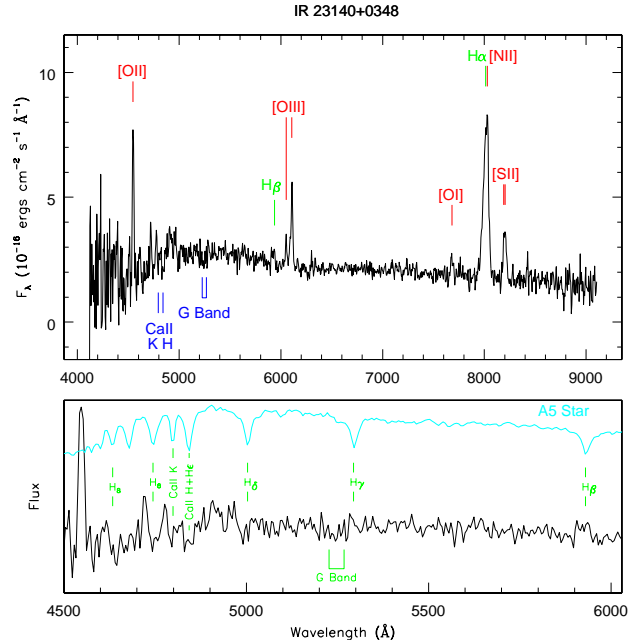


Fig. 14. The top panel shows the optical spectrum for IR 23140+0348. The bottom panel shows a magnified view for the spectral region between 4500Å to 6000Å. For comparison of absorption lines, the spectrum of an A5 star is shown. Prominent lines are labelled.

indicates that IR 23140+0348 has a population of young stars with age ~ 1 Gyr. Combining with the fact that its surface brightness profile is well described by the $R^{\frac{1}{4}}$ law, we conclude that IR 23140+0348 is a young elliptical galaxy resulted from merging. This is further supported by the fact that IR 23140+0348 is a radio galaxy, and such galaxies are often associated with merger remnants (Barnes 1998).

We have also observed three galaxies (G0, G1 and G2 in Fig. 1) in the field of IR 09427+1929. We found that the redshifts for G0 and G2 are 0.284 and 0.149, respectively; the low signal-to-noise ratio and the weak emission features make it difficult to securely identify G1’s redshift. The redshift of G2 is the same as the redshift given for IR 09427+1929 by NED¹. The IRAS error ellipse (see Fig. 1) touches both G0 and G2, with G0 closer to the center of the error ellipse, so the identification is somewhat ambiguous. The spectrum, shown in Fig. 15, indicates that G0 is a narrow line Seyfert 1 galaxy with extremely strong FeII emission. Since almost all extremely strong FeII emitters are ULIRGs, G0 (at $z = 0.284$) is most probably the optical counterpart of the ULIRG. The NED identification seems to have confused the objects G0 and G2. Incidentally

¹ The NASA/IPAC Extragalactic Database (NED) is operated by the Jet Propulsion Laboratory, California Institute of Technology, under contract with the National Aeronautics and Space Administration.

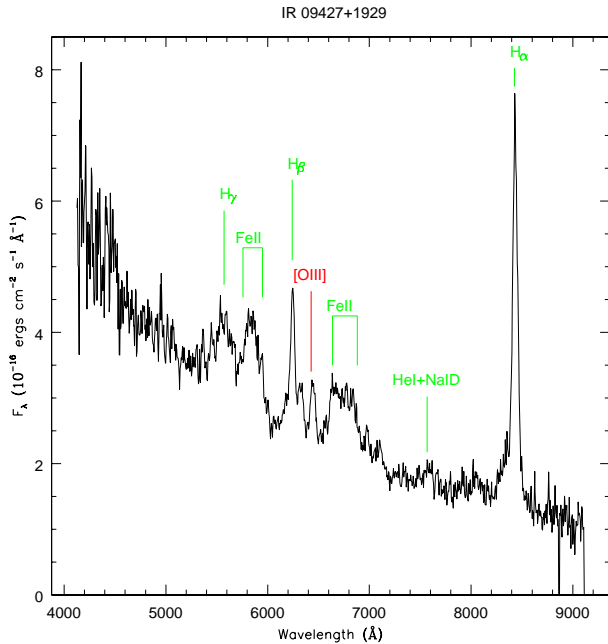


Fig. 15. Spectrum for IR 09427+1929. Prominent lines are indicated. Notice the strong FeII lines.

G2 is a foreground galaxy at $z = 0.149$ with an HII-region like spectrum.

For the other two objects in class I, IR 04025–8303 is also a Seyfert 1 galaxy with FWHM of $H\alpha$ less than 3000 km s^{-1} (Lawrence et al 1999) while the spectral classification for IR 17432–5157 is LINER.

5.2. Class II

As for the spectra of galaxies in Class II, IR 00509+1225 (I Zw 1) is a typical narrow line Seyfert 1 (NLS1) galaxy (Moran et al 1996); IR 10026+4347 is a NLS1-like QSO (Xia et al 1999); IR 00276–2859 is an IR QSO with strong FeII emission line and with FWHM of $H\beta$ about 2000 km s^{-1} ; IR 02055+0835 is also a QSO with strong FeII emission line and the FWHM of $H\beta$ is less than 3000 km s^{-1} from the QDOT redshift survey spectrum obtained by the William Herschel Telescope (Lawrence et al 1999). It is remarkable that all four galaxies in Class II are classified as Seyfert 1 galaxies with strong FeII emission lines and relatively narrow permitted emission lines. Furthermore, the optical luminosities for all four galaxies are in the range of QSOs. Except for IR 02055+0835, all the other three objects were detected in the soft X-ray by ROSAT (the non-detection of IR 02055+0835 is perhaps because it is the most distant galaxy in the sample). All the three soft X-ray spectra are steep. Therefore, these four objects are NLS1-like QSOs (Boller et al 1996), or they are en route to normal QSOs (Xia et al 1999).

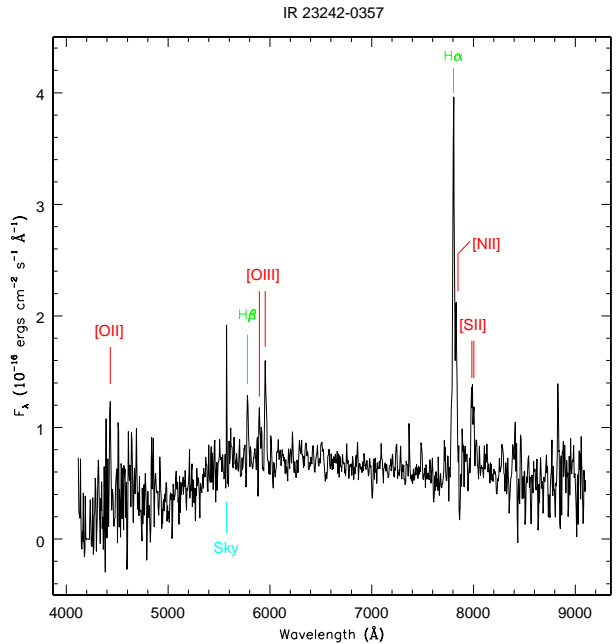


Fig. 16. Spectrum for IR 23242–0357. Prominent lines are labelled.

5.3. Class III

The spectrum for IR 23242–0357 is a typical HII region spectrum (see Fig. 16). Table 2 gives the spectral classifications for the other 4 galaxies in this class based on the data from the literature or the spectra from the QDOT redshift survey. IR 14378–3651 and IR 09039+0503 are classified as LINERs based on Kim et al (1998) and our spectrum (not shown), respectively. As Veilleux et al (1995) pointed out that the excitation mechanism for infrared luminous LINERs could be shock waves. Therefore it is possible that strong shocks are present in IR 14378–3651 and IR 09039+0503, as in some starburst galaxies, such as NGC 6240 and NGC 3690 (Heckman et al 1990). To summarize, the statistical spectral properties of class III objects are very different from those of Class I and Class II. These objects have either HII region-like or LINER-like spectrum, consistent with the presence of starbursts in these galaxies without obvious central AGNs.

6. Summary and Discussions

From a total of 58 HST WFPC2 I-band snapshot images of ULIRGs, we have selected 13 sources that are dominated by a single nucleus to study their surface photometry. According to their surface brightness profiles, we find that these galaxies can be divided into three classes. Below we first briefly summarize their morphology, surface brightness profiles and optical properties, and then discuss the origin and evolution tracks of these galaxies.

The surface brightness profiles of the four galaxies in class I are well fitted by the R^4 law out to $\sim 10h^{-1} \text{ kpc}$.

with bumps at inner few kpc regions. The disk isophotes at the inner region $\lesssim 1h^{-1}$ kpc are consistent with stellar disk formed by infalling gas during merging; molecular disks of comparable size have been detected in CO (e.g., Downes & Solomon 1998). The fine structures at the outer part of these galaxies hints that the relaxation process is incomplete and is slower than the inner part. The large position angle changes also hint that these galaxies are merger remnants and are still evolving into ellipticals. Each member of this class has round appearance. The round appearance suggests that they have experienced multiple mergers, since binary merging tends to produce more elongated objects (Weil & Hernquist 1996). These objects are at the last stage of merging.

The four galaxies in Class II are composed of an inner component described by the $R^{\frac{1}{4}}$ law out to $\sim 5h^{-1}$ kpc plus some outer extension. The existing outer extension indicates that this class of ULIRGs is at intermediate merging stage and the merger remnant has not relaxed completely. On the other hand, the outer extension may be from incompletely relaxed material or they can be stars formed in secondary infall from tidally ejected material (e.g., Barnes 1988).

The five galaxies in class III show various degrees of deviation from the $R^{\frac{1}{4}}$ law, indeed IR 20176–4756 is very well fitted by an exponential law. Except IR 20176–4756, the other four ULIRGs are consistent with their being at an early merging stage, both from their morphologies and surface brightness profiles (see §4.3).

The photometric properties and the optical spectroscopic properties for our ULIRGs seem to be correlated. It is interesting that the percentage of Seyfert 1s is very high (6/13) in our sample compared with complete ULIRG samples, such as Lawrence et al (1999), Kim et al (1998), which has a percentage of Seyfert 1s less than 15%. All class II galaxies are Seyfert 1 galaxies/QSOs while two out of four class I galaxies are Seyfert 1/QSOs as well. At least 5 of these 6 Seyfert 1s /or QSOs are strong or extremely strong FeII emitters and most are NLS1 like galaxies. This is very intriguing since our sample is solely selected using the criterion that there should be a single nucleus from HST snapshot images. In contrast, none of the Class III objects are Seyfert 1s and they are classified as either HIIs or LINERs, which suggests that massive starbursts are present in these galaxies.

Let us now investigate the evolutionary tracks between these three classes of ULIRGs. Morphologically speaking, class I objects are clearly the most relaxed, while class III objects in general show the most disturbed morphologies and photometries, with class II objects somewhere in between. This suggests an evolution sequence from class III to class II, and then to class I, as relaxation proceeds to ultimately form a relaxed elliptical galaxy or S0 galaxies, depending on the initial mass ratios of the merging progenitors (Barnes 1998).

In these three classes of galaxies, the interplay between star formation and central AGN activities is undoubtedly very complex, nevertheless, here we speculate qualitatively on the evolution of these galaxies based on such an interplay. First, as galaxies begin to interact and merge, massive nuclear starbursts are induced. In the mean time, some gas also flows into the center to ignite the central AGN activities, as indicated by numerical simulations. The spectroscopic properties of galaxies at this stage are a composite of the central AGN and circumnuclear starbursts, with the latter being dominating. Our class III objects are probably at this stage. As time goes on, gas continuously fall into the center to fuel more intense central AGN activities, while the star formation has subsided due to the gradual depletion of the gas supply. Most of the dust is blown away, as a result, these galaxies are mostly seen as Seyfert 1 galaxies. As discussed by Xia et al (1999), the Seyfert 1 galaxy with strong FeII emission lines and with steep soft X-ray photon index could be at such a transition stage, namely these objects are emerging young QSOs. Our class II fits this description qualitatively. Finally, as relaxation proceeds even further, gas is mostly consumed by star formation or blown out by superwind (Heckman et al 1990), and the central AGN weakens and the merger remnant emerges as a young elliptical galaxy – our class I objects. If the central gas supply is not yet exhausted, then some of these galaxies can also be Seyfert 1 galaxies (as two of our class I objects are). This picture was first pointed out by Sanders et al (1988a) ten years ago. Our observations seem to confirm this scenario. Along this sequence, the gas behavior is also expected to evolve. There is strong evidence that there are large (ten kpc scale), extended HI or emission-line nebula around some ULIRGs (Armus et al 1990; Hibbard & Yun, 1997). The extended gas distribution is formed by the secondary infall of gas thrown out during the merging process. The infalling gas may form some outer extension of ULIRGs, as seen in our Class II objects. It will be very interesting to obtain HI information to study the evolution of gas in these galaxies (cf. Hibbard & Van Gorkom 1996).

To conclude, from our analysis of the photometry of ULIRGs, we found that these galaxies are excellent laboratories and the surface brightness profile analysis is an important way to study the merging process. The observational data provide a hint that some of these galaxies reside in groups of galaxies and multi-merger is not rare. Six out of these thirteen galaxies are Seyfert 1s or QSOs, strongly suggesting that the AGN phenomenon is universal in the merging process and is an integral part of elliptical galaxy formation. A number of important works remain to be done. A multi-color campaign of these objects will provide invaluable information about the star formation sites and the relative importance of starbursts and central nuclear activities. Furthermore, many galaxies (including a number of small and faint galaxies) are within the field of the primary ULIRGs. Whether these galaxies

are physically associated with the ULIRGs awaits future spectroscopic observations. Such observations will provide insight not only on the environments of ULIRGs but also on the nature of dwarf galaxies around these ULIRGs.

Acknowledgements. We thank Dr. H.J. Mo for useful discussions and the BATC members for data reduction. This project was partially supported by the NSF of China.

References

- Armus, L., Heckman, T.M., & Miley, G.K., 1990, APJ, 364, 471
- Baker, A.C., & Clements, D.L., 1997, IAUS, 186,106
- Barnes, J.E. 1984, MNRAS, 208, 873
- Barnes, J.E. 1985, MNRAS, 215, 517
- Barnes, J.E. 1988, ApJ, 331, 699
- Barnes, J.E. 1989, Nature, 338, 123
- Barnes, J.E. 1992, ApJ, 393, 484
- Barnes, J.E., & Hernquist, L. 1996, ApJ, 471, 115
- Barnes, J.E. 1998, astro-ph/9811242
- Bertin, E., & Arnouts, S. 1996, A&AS, 117, 393
- Boller Th., Brandt W.N., Fink H., 1996, A&A 305, 53
- Borne, K.D., et al 1998, astro-ph/9809040
- Breugel, W.V., 1999, astro-ph/9902048
- Capaccioli, M. 1989, in Corwin H.G., Bottinelli L., eds, The World of Galaxies, Springer-Verlag, Berlin, p.208
- Carter, D. 1977, PhD thesis, University of Cambridge
- Clements, D.L., Sutherland, W.J., McMahan, R.G., & Saunders, W. 1996, MNRAS, 279, 477
- Carollo, C.M., Franx, M., Illingworth, G.D., & Forbes, D.A., 1997, ApJ, 481, 710
- de Zeeuw, T., & Franx, M.1991, ARA&A, 29, 239
- Downes, D., & Solomon, P.M. 1998, ApJ, 507, 615
- Doyon, R., et al 1994, ApJ, 437, 23
- Dressler, A., Gunn, J.E. 1983, ApJ, 270, 7
- Farouki, R.T. & Shapiro, S.L. 1982, ApJ, 259,103
- Heckman, T.M., Armus, L., & Miley, G.K., 1990, ApJS, 74, 833
- Hernquist, L. 1992, ApJ, 400, 460
- Heyl, J., Hernquist, L., & Spergel, D.N. 1994, 427, 165
- Hibbard, J.E. & Yun, M.S. 1997, AAS, 191, 12911
- Hibbard, J.E. & Van Gorkom, J. 1996, AJ, 111, 655
- Hickson, P. 1982, ApJ, 255, 382
- Hickson, P. 1993, Ap. Lett. Comm, 29, 1
- Holtzman, J., et al 1995b, PASP, 107, 156
- Icke, V. 1985, A&A, 144, 115
- Jedrzejewski, R.I. 1987, MNRAS, 226, 747
- Johansson, L., 1991, A&A, 241, 389
- Kim, D.C., Veilleux, S., & Sanders, D.B., 1998, ApJ, 508, 627
- Kormendy, J., & Bender, R. 1996, ApJ, L119
- Lawrence, A. et al 1999, in preparation
- Leech, K.J., et al 1994, MNRAS, 267, 253
- Mamon, G.A. 1987, ApJ, 321, 622
- Marleau, F.R., & Simard, L. 1998, astro-ph/9807223
- Melnick, J., & Mirabel, I.F. 1990, A&A, 231, L19
- Mihos, J.C., & Hernquist L. 1994, ApJ, 431, L9
- Moran, E.C., Halpern, J.P., & Helfand, D.J. 1996, ApJS, 106, 341
- Murphy, T.W., Marrhews, K., Soifer, B.T., Mazzarella, J.M., et al 1996, AJ, 111, 1025
- Negroponte, J. & White, S.D. 1983, MNRAS, 205,1009
- Noguchi, M. 1988, A&A, 203, 259
- Osterbrock, D.E., 1989, In Astrophysics of Gaseous Nebulae and Active Galactic Nuclei, p330
- Saglia, R. P.; Burstein, D., Baggley, G., Bertschinger, E., Colless, M. M., Davies, R. L., McMahan, R. K., JR., Wegner, G. 1997, MNRAS, 292, 499
- Sanders, D.B., & Mirabel, I.F. 1996, ARA&A, 34, 749
- Sanders, D.B., Soifer, B.T., Elias, J.H., Madore, B.F., et al 1988a, ApJ, 325, 74
- Sanders, D.B., et al 1988b, ApJ, 328, L35
- Schweizer, F. 1989, Nature, 338, 119
- Sérsic, J.L. 1968, Atlas de Galaxias Australes (Cordoba: Observatorio Astronomica)
- Springel, V., & White, S.D.M. 1998, astro-ph/9807320
- Surace, J.A, Sanders, D.B., Vacca, W.D., Veilleux, S., and Mazzarella, J.M., 1998, ApJ, 492, 116
- Taniguchi, Y., & Shioya, Y. 1998, ApJ, 501, L167
- Toomre, A. 1977, in The Evolution of Galaxies and Stellar Populations, ed. B. Tinsley & R. Larson (New Haven, CN: Yale Univ. Press), 401
- Toomre, A., & Toomre, J. 1972, ApJ, 178, 623
- Tran, H. D., Brotherton, M. S., Stanford, S. A., van Breugel, W., Dey, A., Stern, D., Antonucci, R. 1998, astro-ph/9812110
- Vader, J. P., & Simon, M. 1987, 327, 304
- Veilleux, S., et al, 1995, ApJS, 98, 171
- Walker, I.R., Mihos, J.C., & Hernquist, L. 1996, ApJ, 460, 121
- Weil, M.L., & Hernquist, L. 1996, ApJ, 460, 101
- White, S.D.M. 1978, MNRAS, 184, 185
- Wu, H., Zou, Z.L., Xia, X.Y., Deng, Z.G. 1998, A&AS, 132, 181
- Xia, X.Y., Mao, S., Wu, H., Zheng, Z., Boller, Th., Deng Z.G., Zou Z.L. 1999, A&A, 341, L13